Icarus 221 (2012) 888–899

Contents lists available at SciVerse ScienceDirect

Icarus

journal homepage: www.elsevier.com/locate/icarus

Regolith grain sizes of Saturn's rings inferred from Cassini–CIRS far-infrared spectra

Ryuji Morishima [a,b,*], Scott G. Edgington [a], Linda Spilker [a]

[a] Jet Propulsion Laboratory, California Institute of Technology, Pasadena, CA 91109, USA
[b] University of California Los Angels, Institute of Geophysics and Planetary Physics, Los Angeles, CA 90095, USA

ARTICLE INFO

Article history:
Received 20 April 2012
Revised 8 August 2012
Accepted 9 September 2012
Available online 3 October 2012

Keywords:
Saturn, Rings
Infrared observations
Radiative transfer
Regoliths

ABSTRACT

We analyze far-infrared (10–650 cm^{-1}) emissivity spectra of Saturn's main rings obtained by the Cassini Composite Infrared Spectrometer (CIRS). In modeling of the spectra, the single scattering albedos of regolith grains are calculated using the Mie theory, diffraction is removed with the delta-Eddington approximation, and the hemispherical emissivities of macroscopic free-floating ring particles are calculated using the Hapke's isotropic scattering model. Only pure crystalline water ice is considered and the size distribution of regolith grains is estimated. We find that good fits are obtained if the size distribution is broad ranging from 1 μm to 1–10 cm with a power law index of ~3. This means that the largest regolith grains are comparable to the smallest free-floating particles in size and that the power law indices for both free-floating particles and regolith grains are similar to each other. The apparent relative abundance of small grains increases with decreasing solar phase angle (or increasing mean temperature). This trend is particularly strong for the C ring and is probably caused by eclipse cooling in Saturn's shadow, which relatively suppresses warming up of grains larger than the thermal skin depth (~1 mm) under subsequent solar illumination.

1. Introduction

Saturn's rings consist of a large number of icy particles. The range of the particle size in the main rings (the A, B, C rings, and the Cassini division) deduced from radio and stellar light occultations is roughly 1 cm to 10 m (Marouf et al., 1983; Zebker et al., 1985; French and Nicholson, 2000; Cuzzi et al., 2009). The composition of ring particles is mostly crystalline water ice and the mass fraction of contaminants (e.g., Tholins, PAHs, or nanohematite) is 10% at most (Epstein et al., 1984; Cuzzi et al., 2009) and probably less than 1% (Poulet et al., 2003). A favorable origin of Saturn's rings with such a high content of water ice is stripping of the icy mantle of a Titan-sized satellite (Canup, 2010). Subsequent meteoritic pollution for 4.5 Gyr may darken the rings too much if the ring mass has been kept similar to the present mass (Cuzzi and Estrada, 1998; Elliott and Esposito, 2011), but initially very massive rings suggested from the Canup's model have not yet been taken into account in pollution models.

Individual ring particles are likely to be covered by regolith grains,[1] probably formed by meteoritic bombardment (Elliott and Esposito, 2011). The regolith grain size is estimated from ring spectra at different wavelengths from ultraviolet to submillimeter ranges, but the estimated size is puzzling as it increases with wavelength. For far-ultraviolet wavelengths, Bradley et al. (2010) estimate the mean photon path length, which is probably the order of the grain size, as 2–5 μm. For near-infrared wavelengths, the estimated grain size varies from author to author (Nicholson et al., 2008; Cuzzi et al., 2009; Filacchione et al., 2012) ranging from 5 to 100 μm, but all these works suggest a relatively smaller size in the C ring than the A and B rings. These works for near-infrared spectra assume that the ring composition is pure water ice, and the size difference could be due to different water bands used or different radiative transfer models. Poulet et al. (2003) study the ring composition using both visible and near infrared spectra. Their model calls for a wide spread in grain sizes: 10–1000 μm for the A and B rings and 30–7500 μm for the C ring. The large difference in the grain size of the C ring from other works indicates that there is some degeneracy between the ring composition and grain size. For far-infrared wavelengths, Spilker et al. (2005) find that the B ring spectrum is well fitted by a model spectrum with the grain sizes ranging from 8 μm to 10 m and the power-law index of 3.4 (the upper limit of 10 m means that the entire ring is considered as regolith layers in their study).

Since Saturn orbit insertion of the Cassini spacecraft in July 2004, the Cassini Composite Infrared Spectrometer (CIRS) has obtained millions of spectra (7 μm to 1 mm) of Saturn's rings (Flasar et al., 2005; Spilker et al., 2005, 2006; Altobelli et al., 2007, 2008, 2009; Leyrat et al., 2008; Flandes et al., 2010, Morishima et al., 2011). Except for Spilker et al. (2005), all above works discuss ring

* Corresponding author at: Jet Propulsion Laboratory, California Institute of Technology, Pasadena, CA 91109, USA.
E-mail address: Ryuji.Morishima@jpl.nasa.gov (R. Morishima).

[1] Throughout the paper, we use "particles" for free-floating particles and "grains" for regolith grains.

0019-1035/$ - see front matter © 2012 Elsevier Inc. All rights reserved.
http://dx.doi.org/10.1016/j.icarus.2012.09.012

temperatures. The signal-to-noise levels of individual spectra are usually good enough to derive temperatures using Planck fits whereas averaging over many spectra are necessary for spectroscopy to examine grain sizes and possible contaminants. In Spilker et al. (2005), only the spectral data in the very early phase of the mission are analyzed. In the present study, using the many spectra we have obtained so far, radial variation and dependence on observational geometries are examined in detail.

In Section 2, we explain how to derive emissivity spectra from observed radiances. In Section 3, selection and averaging of data are discussed. In Section 4, the modeling of emissivity spectra is described. In Section 5, the estimated grain size distributions for different rings are shown. Interpretations of the results and comparison with previous works are discussed in Section 6. The summary of the present work is given in Section 7.

2. Derivation of emissivity spectra from observed radiances

The quantity directly obtained by the spectrometer is the radiance $I(\nu)$ as a function of wavenumber, ν. If the emissivity $\epsilon(\nu)$ is assumed not to vary over a footprint, the form of $I(\nu)$ for ring thermal emission is given as

$$I(\nu) = \epsilon(\nu)\beta_{\rm geo}\int f(T)B(T,\nu)dT, \tag{1}$$

where $\beta_{\rm geo}(\leqslant 1)$ is the geometric filling factor of a ring (see Section 2.4), $f(T)$ is the distribution function of temperature T inside a footprint, normalized as $\int f(T)dT = 1$, and $B(T,\nu)$ is the Planck function. Because the temperature inside the footprint is not known and may not be uniform, it is not straightforward to derive $\epsilon(\nu)$ from $I(\nu)$, unlike temperature-controlled laboratory measurements. With different assumptions, different types of emissivities are obtained. Three different emissivities are introduced in the following: $\epsilon_0(\nu)$ derived by a fit with a single temperature, $\epsilon_1(\nu)$ derived by a fit with two temperatures, and $\epsilon_2(\nu)$ derived by a fit with two temperatures and an expected emissivity spectrum.

2.1. Fits with a single temperature

If the temperature distribution is represented by a single effective temperature T_0, one may have

$$\int f(T)B(T,\nu)dT = \beta_{\rm therm}(\nu)B(T_0,\nu), \tag{2}$$

where $\beta_{\rm therm}$ is the correction factor due to multiple temperatures inside a footprint. The expected shape of $\beta_{\rm therm}$ is discussed in Section 2.2.

In the first method to obtain the emissivity is to assume $\beta_{\rm therm}(\nu) = 1$. Substituting Eq. (2) into Eq. (1), we obtain

$$\epsilon_0(\nu) = \frac{I(\nu)}{\beta_{\rm geo}B(T_0,\nu)}. \tag{3}$$

The temperature T_0 is obtained by minimizing the residuals R_0

$$R_0(T_0,\epsilon_{\rm sca,0}) = \sum_\nu\left(\frac{I(\nu)-\epsilon_{\rm sca,0}\beta_{\rm geo}B(T_0,\nu)}{\sigma(\nu)}\right)^2, \tag{4}$$

where $\epsilon_{\rm sca,0}$ is the (scalar) emissivity averaged over wavelengths and $\sigma(\nu)$ is the instrument noise equivalent spectral radiance (NESR; see Flasar et al., 2004). The above Planck fits are applied to all CIRS ring spectra to obtain corresponding temperatures. In Spilker et al. (2005), Eqs. (3) and (4) are used and $\epsilon_0(\nu)$ is averaged over many spectra. Altobelli et al. (2008) estimated $\epsilon_{\rm sca,0}$ for the C ring to be ~0.9. It is expected that Eq. (4) works well if the temperature variation in the footprint is small ($\beta_{\rm therm}(\nu)\simeq 1$) and $\epsilon(\nu)$ is roughly flat over wavelength of interest.

2.2. Fits with two temperatures

It is unlikely that the temperature inside a single footprint is perfectly uniform. The particle temperature may vary radially and vertically. Even on the surface of a single particle, large temperature variation may exist as the temperature is expected to be highest and lowest around the sub-solar and anti-sub-solar points, respectively. Instead of deriving a temperature distribution with complicated thermal models which calculate the energy balance of rings, simply two portions with high and low temperatures ($T_{\rm w1}$ and $T_{\rm c1}$) are considered:

$$\int f(T)B(T,\nu)dT = f_{\rm w1}B(T_{\rm w1},\nu) + (1-f_{\rm w1})B(T_{\rm c1},\nu), \tag{5}$$

where $f_{\rm w1}$ is the fraction of the warm portion. Fits with two temperatures are also used in analysis of thermal emission of icy satellites (Carvano et al., 2007; Howett et al., 2011). Substituting Eq. (5) into Eq. (1), the emissivity is given by

$$\epsilon_1(\nu) = \frac{I(\nu)}{\beta_{\rm geo}[f_{\rm w1}B(T_{\rm w1},\nu) + (1-f_{\rm w1})B(T_{\rm c1},\nu)]}. \tag{6}$$

As in Eq. (4), the temperatures and factors are determined by minimizing the residual as

$$R_1(T_{\rm w1},T_{\rm c1},\epsilon_{\rm sca,1},f_{\rm w1}) = \sum_\nu\left(\frac{I(\nu)-\epsilon_{\rm sca,1}\beta_{\rm geo}[f_{\rm w1}B(T_{\rm w1},\nu)+(1-f_{\rm w1})B(T_{\rm c1},\nu)]}{\sigma(\nu)}\right)^2, \tag{7}$$

where $\epsilon_{\rm sca,1}$ is the scalar emissivity. For the convenience of later use, we also define the relative emissivity $\epsilon_{\rm rel,1}(\nu)$ as

$$\epsilon_{\rm rel,1}(\nu) = \frac{\epsilon_1(\nu)}{\epsilon_{\rm sca,1}}. \tag{8}$$

The relative emissivity is roughly scaled to be unity, so is suitable for comparison between different spectra.

Equating Eqs. (2) and (5), the form of $\beta_{\rm therm}$ is given as

$$\beta_{\rm therm}(\nu) = \frac{f_{\rm w1}B(T_{\rm w1},\nu) + (1-f_{\rm w1})B(T_{\rm c1},\nu)}{B(T_0,\nu)}. \tag{9}$$

An example of $\beta_{\rm therm}$ for various values of $f_{\rm w1}$ is shown in Fig. 1. Near the Planck peak (~200 cm^{-1}), $\beta_{\rm therm}$ takes the lowest value

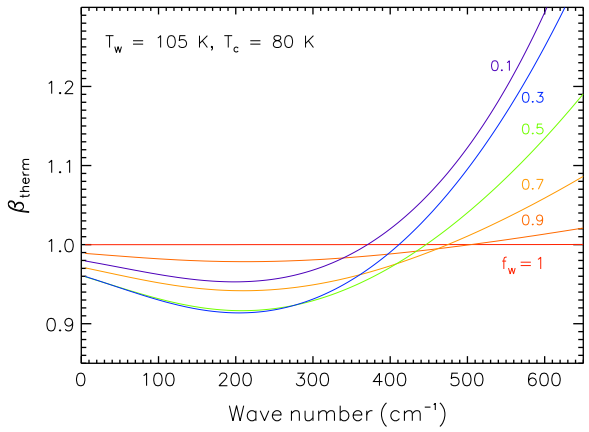

Fig. 1. Examples of $\beta_{\rm therm}$ as a function of ν, given by Eq. (9). Here we adopt $T_{\rm w1}$ = 105 K and $T_{\rm c1}$ = 80 K, and T_0 is obtained from a Planck fit (Eq. (4)). Different colors represent different values of the fraction of the warm portion, $f_{\rm w1}$. (For interpretation of the references to color in this figure legend, the reader is referred to the web version of this article.)